06

Strength properties, mechanisms of high-speed plastic deformation and failure of Ti-6Al-3Mo alloy in shock waves

© A.V. Pavlenko,[1] A.V. Dobromyslov,[2] N.I. Taluts,[2] S.N. Malyugina,[1] S.S. Mokrushin,[1] M.S. Mytarev,[1] M.A. Borshchevsky[1]

[1]Russian Federal Nuclear Center — Zababakhin All Russia Research Institute of Technical Physics, 456770 Snezhinsk, Chelyabinsk region, Russia
[2]M.N. Mikheev Institute of Metal Physics, Ural Branch, Russian Academy of Sciences, 620108 Yekaterinburg, Russia
e-mail: dep5@vniitf.ru

Received March 31, 2025
Revised March 2, 2025
Accepted June 6, 2025

The results of measuring the shock compression wave profiles of samples $(\alpha+\beta)$ of titanium alloy Ti-6Al-3Mo under different shock wave loading conditions are presented, as well as the results of metallographic examination of samples preserved after loading. The dependences of the deflection strength on the rate of deformation in the rarefaction wave and the Hugoniot elastic limit on the propagation time of the compression wave in the material are obtained. The values of Hugoniot's deflection strength and elastic limit were determined in the temperature range from $-168\,^{\circ}$C to $400\,^{\circ}$C. The results of metallographic studies of the preserved samples showed that under the realized loading conditions, high-speed plastic deformation is carried out by sliding, and the formation of twins does not occur. A characteristic feature of the high-speed plastic deformation of the alloy under study was the formation of bands of strain localization, and mechanical failure occurred through the formation of deflection and shear cracks.

Keywords: $(\alpha+\beta)$-titanium alloy, shock wave effect, deflection strength, Hugoniot elastic limit, deformation rate, high-speed plastic deformation, structure.

DOI: 10.61011/TP.2025.11.62241.54-25

Introduction

Titanium alloys have a unique combination of physical and mechanical properties that provide them with a wide range of applications in various fields of industry. They occupy a special place in aviation and space technology, where special requirements are placed on structural materials. In this regard, much attention is paid to the study of the properties of titanium alloys [1–15].

Depending on the phase composition, titanium alloys are conventionally divided into five groups: α-, pseudo-α, two-phase $(\alpha+\beta)$-, pseudo-β- and β-alloys. Two-phase $(\alpha+\beta)$ alloys (VT6, VT8, VT9, VT14) have the highest strength and high thermal stability. Alloys of this group have a lamellar structure, which consists of α-phase slats and β-phase interlayers (slats) between them. Such a structure can affect both the dynamic properties and the mechanisms of high-speed plastic deformation and fracture during shock wave loading.

There are a number of papers devoted to studies of the dynamic properties of titanium alloys $(\alpha+\beta)$ of the [4,12–15] group, while not all of them provide data on the deformation structure after impact [12,14,15].

The effect of test temperature on the dynamic properties of $(\alpha+\beta)$-alloy Ti-6Al-2Sn-2Zr-2Cr-2Mo-Si was studied in [4]. It has been found that dynamic strength is much less sensitive to alloy composition, structure, and test temperature than yield strength. As the temperature increases, the amplitude of the elastic precursor decreases, and the increase in parameters behind its front becomes steeper, while the steepness of the plastic compression wave practically does not change. The deflection strength is maximal at room temperature (4.8 GPa) and decreases monotonously with increasing and decreasing temperatures.

The dependence of the deflection strength $(\alpha+\beta)$ of the VT6 alloy on the deformation rate at room temperature was obtaned in [13] in the range from $1\cdot10^4$ to $1.9\cdot10^6\,\mathrm{s}^{-1}$, approximated by a power function. The deflection strength ranged from 4.1 to 5.1 GPa. An increase in temperature from 20 °C to 600 °C leads to a decrease in the dynamic elastic limit. The deformation structure of the samples was not studied.

The study of preserved samples $(\alpha+\beta)$ of VT6 and VT14 alloys in [12] revealed the formation of shear bands (bands of strain localization) and a new type of mesodefects — screw rotations. The maximum deflection strength corresponds to the maximum density of screw rotations. It is noted in Ref. [14] that dislocation sliding is the predominant mechanism of deformation in the Ti-6Al-4V alloy (an analog of the VT6 alloy). At the same time, flat clusters of dislocations were revealed in the lamellar structure. A small number of twins are formed when the thickness of the α-phase plates is $2\,\mu$m.

It was shown in [15] when studying the alloy Ti-6Al-4V with a different initial structure consisting of equiaxed grains of α- and β-phases that high-speed deformation at the speed of $5 \cdot 10^3\,\mathrm{s}^{-1}$ occurs with the formation of flat clusters of dislocations and numerous twins. It is also shown that with an increase in the initial temperature to 222 °C at a velocity of $0.001\,\mathrm{s}^{-1}$, the deformation mechanism changes to a more chaotic sliding.

VT8 alloy (Ti-6Al-3Mo) is used for the manufacture of critical parts such as discs and blades of gas turbine aircraft engines and parts for various purposes operating at temperatures up to 480 °C. At the same time, there is very little data in the literature on the dynamic properties and mechanisms of deformation and fracture of VT8 alloy.

In order to compensate for the lack of experimental data, this paper presents the results of a study of the elastoplastic and strength properties, as well as the mechanisms of high-speed plastic deformation and fracture of the VT8 alloy under shock wave action in a wide range of deformation rates, loading intensity and variations in the initial temperatures of the samples.

1. Experimental technique

Samples cut from a rod in the form of discs with a diameter of 34 mm and thicknesses from 0.5 to 4 mm were studied. The faces of the samples were sanded to remove surface defects and obtain the necessary plane parallelism. Chemical composition of VT8 alloy (mass%): Ti — main, Al — (5.8–7), Mo — (2.8–3.8), Zr — 0.5, Si — (0.2–0.4), Fe — 0.3, O — 0.15, H — 0.015, other impurities — 0.3.

The samples were subjected to intense shock wave action in experiments on a single-stage light gas cannon with a caliber of 44 mm [16]. A flat impactor made of VT8 alloy, mounted on a piston, accelerated in the barrel of a light-gas cannon and collided with the test sample. At this moment, a shock wave process occurred in the sample-impactor system in the form of propagation of flat one-dimensional compression and rarefaction waves, which was recorded as a change in the velocity of the free surface of the sample. The velocity of movement of the free surface was recorded using the VISAR [17] and PDV [18] laser interferometric methods. Based on the obtained velocity profiles, the values of the deflection strength and the elastic limit of Hugoniot were calculated.

The speed of the collision was determined using electrical contact sensors, which also made it possible to control the skew of the collision. The accuracy of measuring the impact velocity was 0.2 % [16]. Laser methods have a velocity measurement accuracy of 1 % and a time resolution of ~ 2 ns.

The initial temperature of the samples was varied in the range from −168 °C to 400 °C. Liquid nitrogen was used for cooling. An induction heater was used in experiments at a high temperature of the test sample. The temperature was controlled using a thermocouple with an accuracy of ±5 °C.

The samples preserved after shock wave loading were examined using optical metallography, X-ray diffraction analysis, and scanning electron microscopy (SEM). Microhardness was also measured. X-ray diffraction analysis was performed on a DRON-3 diffractometer using Cu Kα radiation and a graphite crystal monochromator, optical metallography — on a microscope Neophot-30, electron microscopic examination — using a Quanta 200 scanning electron microscope. The microhardness was measured on a PMT-3 microhardness tester at a load of 0.98 N.

2. Results of the study

According to X-ray diffraction analysis, VT8 alloy in its initial state is two-phase and consists of α- and β-phases. The lattice periods α-phases are $a_\alpha = (0.2927 \pm 0.0001)$ nm, $c_\alpha = (0.4672 \pm 0.0001)$ nm, $c/a = 1.596$. The lattice period β is the phase $a_\beta = (0.3246 \pm 0.0001)$ nm.

The initial structure of the alloy has a lamellar structure consisting of α-phase slats and β-phase interlayers (Fig. 1). Aluminum and zirconium are mainly found in the crystal lattice of the α phases, while molybdenum and iron are found in the interlayers of the β phases. In the image obtained by optical metallography, the α-phase has a light contrast, and the β-phase has a dark contrast (Fig. 1, *a*). In the image obtained using a scanning electron microscope, the contrast is opposite (Fig. 1, *b*). The thickness of the α-phase slats averages 1.6 μm, and the thickness of the β-phase interlayers averages 0.4 μm.

The value of the microhardness of the alloy in the initial state $H_\mu = (3407 \pm 73)$ MPa. VT8 alloy has a density of $\rho_0 = 4430\,\mathrm{kg/m^3}$. The longitudinal and shear sound velocities measured by ultrasound are $C_l = (6100 \pm 16)$ m/s and $C_s = (3130 \pm 16)$ m/s, respectively, and the calculated volumetric sound velocity is $C_b = (4910 \pm 16)$ m/s.

The primary results of shock wave experiments are shown in Fig. 2 in the form of velocity profiles of the free surface of the samples. The velocity profiles in Fig. 2, *a* were obtained at impact velocities from 408 to 1083 m/s, which corresponds to the pressure range in shock waves from 4.6 to 13.2 GPa. The thickness of the samples in these experiments was 4 mm, the thickness of the impactor was 2 mm, the initial temperature of the samples was room temperature. The impact velocity in m/s is indicated next to each profile. A two-wave configuration of the shock wave is recorded on all profiles with the release of an elastic precursor and a plastic compression wave following it due to the difference in the propagation velocities of longitudinal elastic perturbations and a plastic deformation wave. The plastic shock wave is followed by a plateau of stationary flow, an unloading wave, a deflection pulse, and subsequent reverberation of waves in the deflection plate. On the profile corresponding to the impact velocity

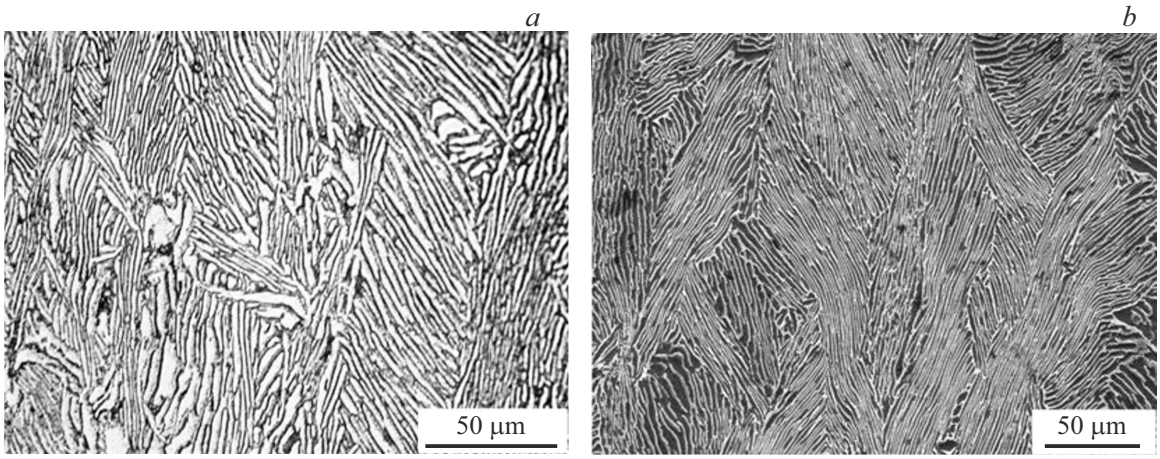

Figure 1. The structure of VT8 alloy in its initial state: *a* — optical metallography; *b* — scanning electron microscopy.

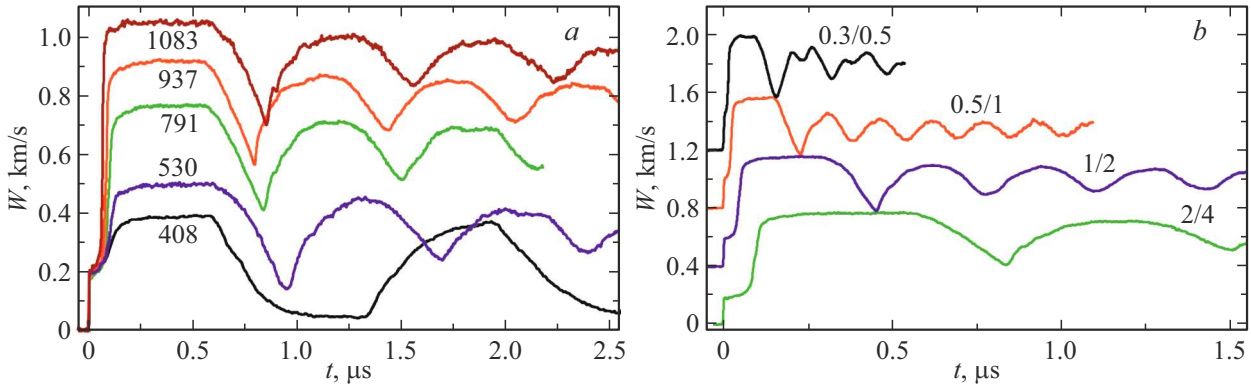

Figure 2. . Velocity profiles of the free surface of VT8 alloy samples at normal initial temperature: *a* — with variations in the intensity of the shock wave; *b* — with variations in the duration of the loading pulse.

(408 ± 0.8) m/s (corresponding pressure behind the shock wave front — 4.6 GPa), no breakage was recorded, since the magnitude of the tensile stress does not exceed the deflection strength. A delay of the moment when the deflection pulse reaches the free surface is observed on the velocity profile corresponding to the impact velocity (1083 ± 2) m/s (13.2 GPa). This delay may be caused by the $\alpha \rightarrow \omega \rightarrow \alpha$-phase transformation. It is not possible to establish the exact pressure limit of the beginning of the $\alpha \rightarrow \omega$-junction, since there is no clear separation of the phase precursor at the front of the compression wave, as, for example, for technically pure titanium [10, 11]. It can be argued that the phase transition occurs in the range of impact velocities 937 – 1083 m/s, which corresponds to the pressure range from 11.2 to 13.2 GPa.

In the experiments, the results of which are shown in Fig. 2, *b*, the values of the impact velocities were as follows: for 0.3/0.5 — (799 ± 1.6) m/s, 0.5/1 — (791.3 ± 2.4) m/s, 1/2 — (792 ± 1.6) m/s, 2/4 —(791.1 ± 1.6) m/s. The initial temperature was at room temperature, and only the duration of the loading pulse varied due to changes in the thickness of the impactors and samples. The nominal thickness values of the impactor/sample are indicated above each velocity profile in millimeters. For clarity, the profiles are shifted vertically relative to each other by 400 m/s. The figure shows how the wave profiles evolve with variations in the duration of the loading pulse. With its increase, the duration of the effect of tensile stresses in the sample also increases, which leads to a decrease in the rate of deformation in the rarefaction wave, as evidenced by a decrease in the angle of inclination of the velocity profile section corresponding to the rarefaction. Based on the results of this series of experiments, the dependence of the deflection strength on the rate of deformation in the rarefaction wave was constructed.

In a separate series of experiments, the effect of the initial temperature of the samples on the elastic-plastic and strength properties of the alloy was investigated. Fig. 3 compares the wave profiles obtained when the initial temperature of the studied samples changes. The profiles are shifted in time by 0.3 μs for visual representation. In these experiments, the thicknesses of the impactors were 2 mm, the samples — 4 mm, the impact velocities were approximately the same and were (545.3 ± 1.1) m/s,

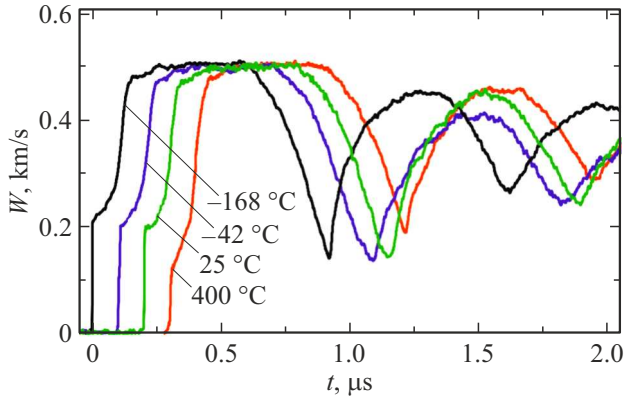

Figure 3. Comparison of free surface velocity profiles of VT8 titanium alloy samples at different initial temperatures.

(544.1 ± 1.1) m/s, (530 ± 1.1) m/s, (532 ± 1.1) m/s at the initial temperatures of the samples $-168\,^{\circ}$C, $-42\,^{\circ}$C, $25\,^{\circ}$C, $400\,^{\circ}$C, respectively. It can be seen that an increase in temperature from room temperature to $400\,^{\circ}$C leads to a decrease in the amplitude of the elastic precursor W_{HEL} and the magnitude of the decrease in surface velocity ΔW from the average value on the plateau to its minimum value before the deflection pulse front, which indicates a decrease in Hugoniot's elastic limit and deflection strength:

$$\sigma_{\mathrm{HEL}} = 0.5\rho_0 C_l W_{\mathrm{HEL}},$$

$$\sigma_{sp} = 0.5\rho_0 C_b(\Delta W + \delta),$$

where δ is the correction for the distortion of the velocity profile due to the difference in the propagation velocities of the deflection pulse and the discharge wave [19].

When the temperature decreases to $-168\,^{\circ}$C, Hugoniot's elastic limit and deflection strength practically do not change. The time interval between the release of the elastic precursor and the plastic wave on the free surface is maintained over the entire temperature range. This indicates that the velocity difference between elastic and plastic compression waves in the VT8 alloy persists with temperature changes.

Based on the obtained velocity profiles, the dependence of the deflection strength on the rate of deformation in the rarefaction wave, as well as the dependence of the Hugoniot elastic limit on the distance traveled by the wave in the material, were calculated and constructed (Fig. 4). The values of Hugoniot's elastic limit and deflection strength in the experiment with heating the sample to $400\,^{\circ}$C are highlighted by shading.

The calculated values of the deflection strength are described by empirical dependence: $\sigma_{sp} = 2.69(\varepsilon)^{0.046}$, where ε is the rate of deformation in the rarefaction wave. The attenuation of Hugoniot's elastic limit as a function of the distance h traveled by the wave in the material is described by the ratio $\sigma_{\mathrm{HEL}} = 2.86(h)^{-0.06}$.

„Empty" points in Fig. 4 „deviate" from the general dependence, namely, an increase in deflection strength is observed. These values were obtained by processing the results of experiments in which the pressure in the shock wave was higher than 11.2 GPa (velocity profiles are not given in this work). An increase in the fracture stress is another proof that a $\alpha \rightarrow \omega$-transformation occurs in the alloy. It was shown in [10] that technically pure titanium in the ω-phase has a higher deflection strength than in the α-phase.

For structural studies, three samples were selected, preserved after a single shock compression at room temperature, lowered to $-80\,^{\circ}$C and increased to $400\,^{\circ}$C under fixed loading conditions, at which the impact velocity of the impactor from the samples was about 530 m/s (impact compression pressure in the samples — 6.1 GPa), and one sample stored after loading at the impact velocity (937 ± 1.8) m/s (11.2 GPa) at room temperature.

X-ray diffraction analysis shows that the phase composition of the alloy after shock wave loading did not change under any of the realized loading modes. The diffraction peaks from only the α and β-phases are present on the obtained diffraction patterns.

Under all loading conditions, main cracks form in approximately the average thickness of the sample. However, their appearance significantly depends on the loading mode. Thus, after loading at a velocity of (537 ± 1.1) m/s (6.2 GPa) at $T = -80\,^{\circ}$C, two cracks are found in the sample. The more open crack is located at a distance of ~ 1.5 mm, and the less open crack is located at a distance of ~ 2.5 mm from the upper surface of the slot (Fig. 5, *a*). Since, when loading the sample, the maximum effective longitudinal stresses were in its central part, crack opening occurred mainly in this area, and in the peripheral region cracks remained in an undisclosed state due to lateral unloading.

All defects (pores and small cracks) are concentrated in a strip about 1.2 mm wide in the middle part of the slot. Both cracks are not continuous, but consist of a large number of

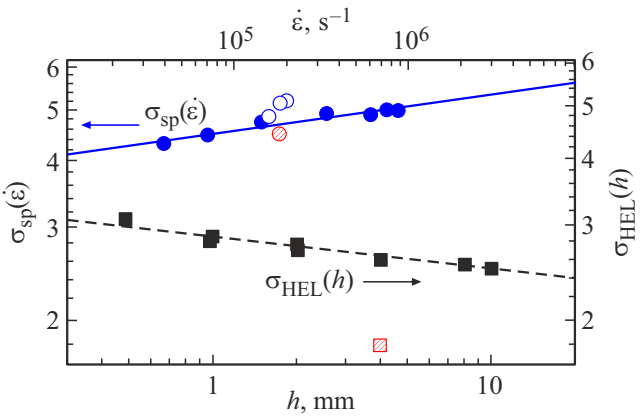

Figure 4. Dependence of the deflection strength $\sigma_{sp}(\varepsilon)$ of the VT8 titanium alloy on the rate of deformation in the rarefaction wave (top) and the dependence of the dynamic elastic limit $\sigma_{\mathrm{HEL}}(h)$ on the distance traveled by the wave in the sample material (bottom); red symbols indicate data when heated to $400\,^{\circ}$C.

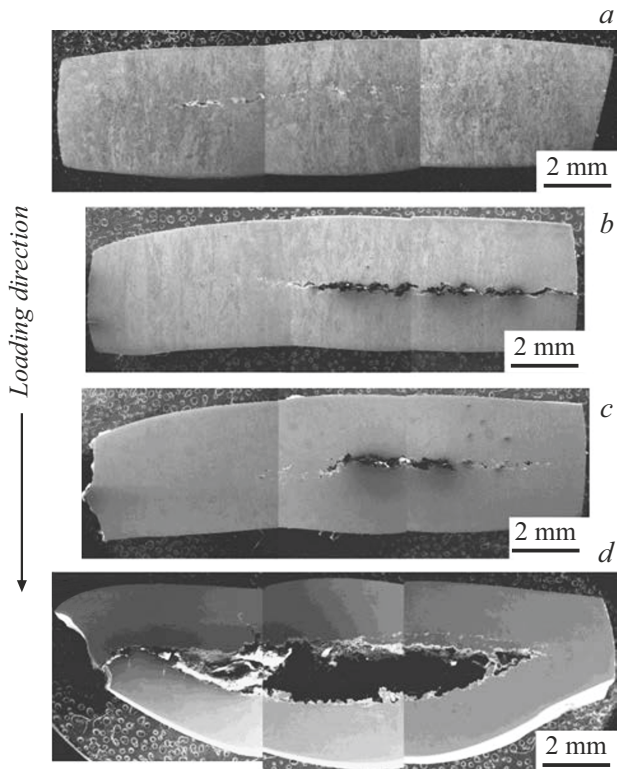

Figure 5. Panoramic cross-sectional images of VT8 alloy samples after various loading modes obtained in a scanning electron microscope: *a* —$V = (537 \pm 1.1)$ m/s, $T = -80\,^{\circ}$C; *b* — $V = (539 \pm 1.1)$ m/s, room temperature; *c* — $V = (532 \pm 1.1)$ m/s, $T = 400\,^{\circ}$C; *d* —$V = (937 \pm 1.8)$ m/s, room temperature. The center of the discs is on the right side.

small deflection and shear cracks and pores (Fig. 6). It is very likely that the formation of fractures of the deflection and shear type in some cases began from one center. This follows from the fact that most large pores (open cracks) have a shape close to a parallelogram, one side of which is perpendicular to the direction of propagation of the shock wave, and the other is located at approximately an angle of 45°. In addition, there are *Z*-shaped cracks in the alloy structure, which were previously observed after shock wave loading in the VT14 alloy in[12].

The formation of split cracks occurred through the nucleation and growth of pores. This is evidenced by the presence of strongly opened cracks and large pores of a dimpled pattern on the surface (Fig. 6, *b*).

When loaded with $V = (530 \pm 1.1)$ m/s (6.1 GPa) at room temperature, only one main crack forms in the sample in the middle section (Fig. 5, *b*). Compared to loading at $T = -80\,^{\circ}$C, it is more open. Due to the greater opening of the crack, the shape of the „parallelograms“ is less pronounced. The crack does not reach the edges of the disk; at the ends it looks like smaller and thinner deflection and shear cracks, which are located at an angle of 45° to the direction of propagation of the shock wave (Fig. 7). The rack-and-pinion nature of the initial structure does not significantly affect the direction of crack propagation (Fig. 7, *c*).

When loaded with $V = (532 \pm 1.1)$ m/s (6.15 GPa) at $T = 400\,^{\circ}$C, only one main crack also forms in the sample (Fig. 5, *c*), which does not reach the edges of the disk, passing into bands of strain localization and pores (Fig. 8, *a*). In some cases, the pores formed as a result of the opening of shear cracks take the form of squares, the sides of which form angles of 45° with the direction of propagation of the shock wave (Fig. 8, *b*).

The greatest opening of the main crack occurs under loading with $V = (937 \pm 1.8)$ m/s (11.2 GPa) (the highest kinetic energy of the circumferential plate) at room temperature (Fig. 5, *d*). The resulting crack passes through almost the entire sample. There is also an undiscovered crack in the upper half of the sample in its middle part, which is observed in the form of a chain of pores. In many cases, the surface of the pores has a characteristic „dimpled pattern“ (Fig. 9).

A characteristic feature of the high-speed plastic deformation of VT8 alloy is the complete absence of twins. The deformation is carried out only by sliding. In many cases, the slats have a toothed appearance (Fig. 10), which indicates the sliding process in both the α-phase and the β-phase. The serration of the boundaries increases both with increasing temperature (Fig. 10, *b*) and with increasing collision velocity (Fig. 10, *c*, *d*).

A similar serration is observed in the images of the structure of VT6 and VT14 alloys after shock wave loading in [12], however, the authors did not pay attention to this fact.

In the process of shock wave loading, deformation localization bands are formed in this alloy. Under loading conditions with $V = (537 \pm 1.1)$ m/s at $T = -80\,^{\circ}$C and $V = (530 \pm 1.1)$ m/s at room temperature, strain localization bands are rarely detected. They often have only a rudimentary form and a small extent (Fig. 11, *a*, *b*). The largest number of strain localization bands is observed after loading at a velocity of (532 ± 1.1) m/s at $T = 400\,^{\circ}$C (Fig. 11, *c*, *d*). At room temperature at the impact velocity $V = (937 \pm 1.8)$ m/s bands of deformation localization are practically absent.

Deformation localization bands are formed both near the main crack and outside it (Fig. 11, *c*). The slats of the α and β-phases near the deformation localization bands bend strongly, and the distance between them decreases significantly, which indicates large shear displacements of the material.

The measurement of microhardness after shock wave loading for all samples was carried out on their cross-sections in the direction from the loading surface to the free surface approximately 1/2 radius from the center of the disk. The obtained average values of the microhardness are shown in the table.

It is established that the greatest increase in the microhardness value is observed at a shock wave loading pressure of the order of 6.2 GPa and, compared with the

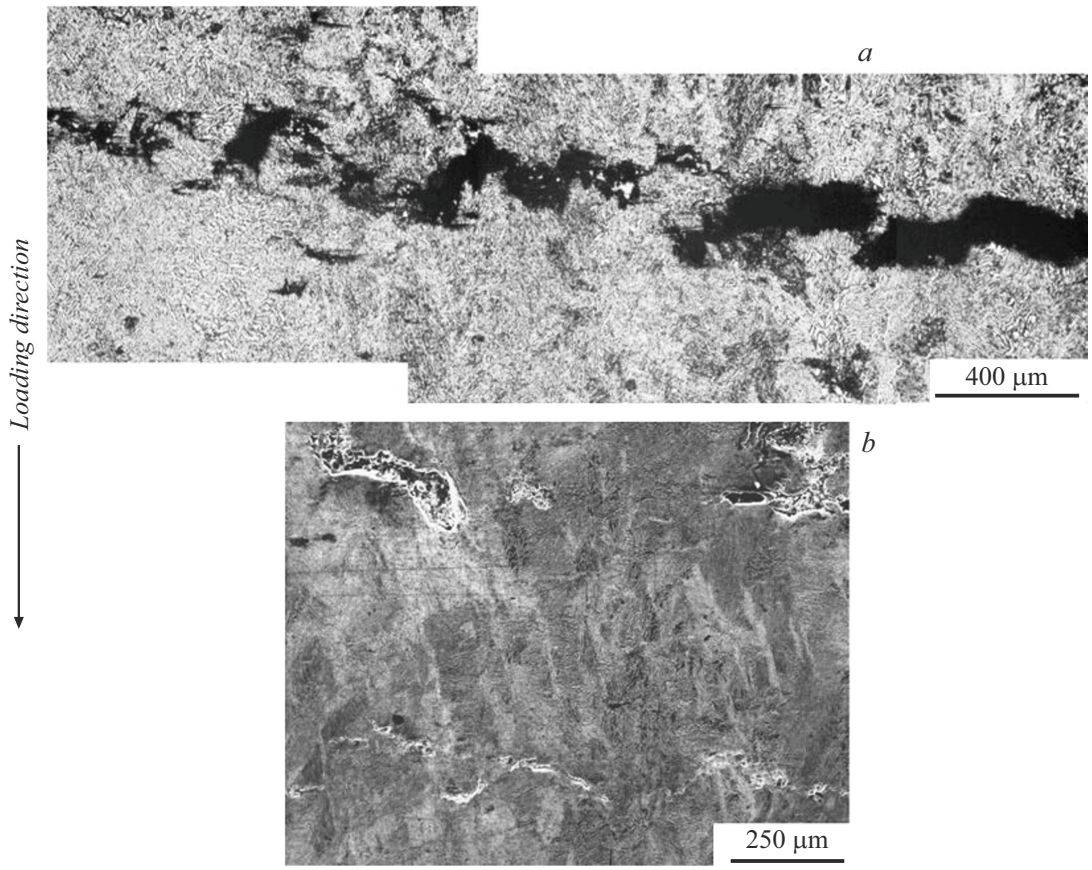

Figure 6. Upper crack (a) and crack fragments (b) in the cross-section of the VT8 alloy sample after loading with $V = (537 \pm 1.1)$ m/s at $T = -80°C$: a — optical metallography; b — scanning electron microscopy.

microhardness of the alloy in its initial state, is 14 %. It should be noted that when the temperature of the samples under study varies, the microhardness value varies within the measurement error. With an increase in the amplitude of the shock wave effect to 11.2 GPa, an increase in microhardness from the initial state was recorded by only 11 %, which may be due to the processes of phase recrystalization.

3. Discussion of the research results

VT8 alloy has significantly higher Hugoniot elastic limit values compared to technically titanium grades VT1-0 [10] and VT1-00 [11]. As the temperature increases, the amplitude of the elastic precursor in the VT8 alloy tends to decrease. Thus, at $T = 400\,°C$, its value is 37 % lower than at $T = 25\,°C$; at the same time, when the temperature drops to $-168\,°C$, it practically does not change.

The shear strength of the studied alloy in the range of strain rates from $\sim 4 \cdot 10^4\,s^{-1}$ to $\sim 10^6\,s^{-1}$ demonstrates a monotonous increase from 4.2 to 5.0 GPa, in contrast to the dependence for titanium VT1-0 in the state of α-phase having a region of sharp increase in deflection strength in the pressure range from 3.7 to 4.9 GPa with a change in the deformation rate from $\sim 1.8 \cdot 10^5\,s^{-1}$ to $\sim 2.1 \cdot 10^5\,s^{-1}$ [10].

The difference between the initial structure of the VT8 alloy and the structure of titanium VT1-0 and VT1-00 has a significant effect on both the fracture mechanism and the mechanism of high-speed plastic deformation. The development of main cracks in VT8 alloy samples occurs through the formation of both flared microcracks resulting from the nucleation and growth of small pores, and microcracks having a shear nature. The greatest number and the greatest extent of shear microcracks are observed in the alloy after loading at a temperature of $T = 400\,°C$.

In titanium, twinning, along with sliding, is the main mechanism of high-speed plastic deformation [5,10,11]. In contrast, in VT8 alloy, sliding is the only deformation mechanism. There is completely no twinning in VT8 alloy. This is due to the small thickness of the α- and β-phase slats. As noted above, the thickness of the α-phase slats averages 1.6 μm, and the thickness of the β-phase interlayers — 0.4 μm. It is known that when the grain size is below the critical level, the formation of twins does not occur [20]. It was shown in [21] that in titanium, at a grain size of 1,μm, twins practically do not form during plastic deformation by rolling. It was found in [14] that only a small number of

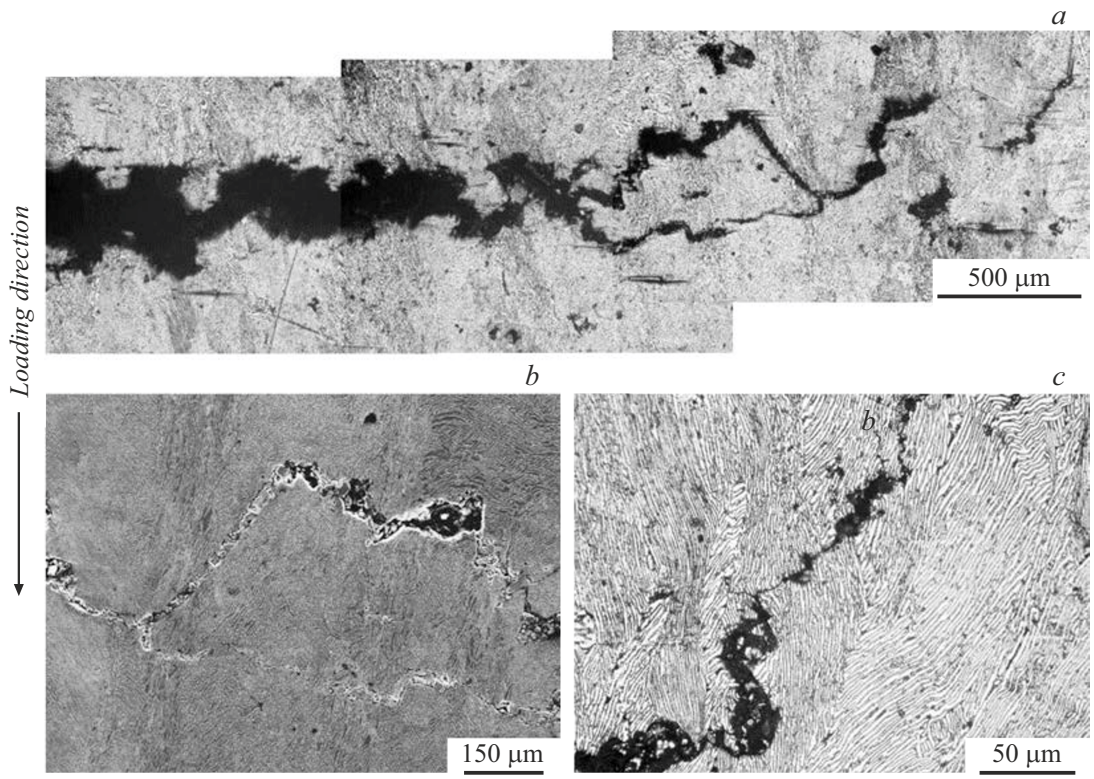

Figure 7. Main crack (a) and small cracks at its ends (b, c) in a sample of VT8 alloy after loading with $V = (530 \pm 1.1)$ m/s at room temperature: a, c — optical metallography; b — scanning electron microscopy.

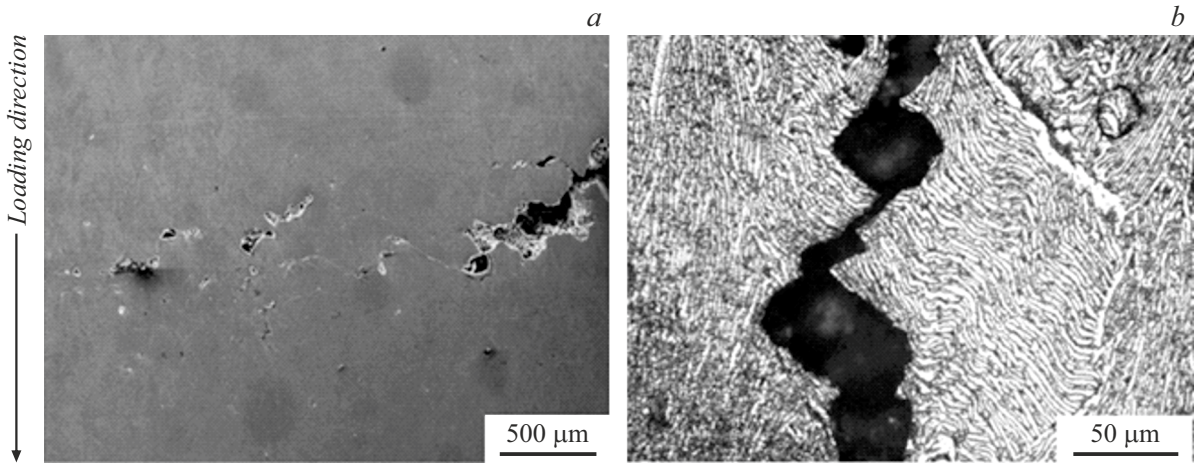

Figure 8. Deformation localization bands and pores at the end of the main crack (a) and pores on the shear crack (b) in the VT8 alloy sample after loading with $V = (532 \pm 1.1)$ m/s at $T = 400\,^{\circ}$C: a — scanning electron microscopy; b — optical metallography.

twins were formed during shock wave loading of the alloy Ti-6Al-4V with a lamellar microstructure at a width of α-plates $\sim 2\,\mu$m, and no twins were observed with the smaller width of α-plates.

The studied alloy consists of α-phase and β-phase. The alpha phase has a HCP crystal lattice, and the β-phase has a BCC crystal lattice. The predominant sliding plane in the α-phase under normal deformation conditions is the prismatic plane $\{10\bar{1}0\}$ [22,23]. Sliding along the reference plane (0001) is also possible. Sliding in both planes occurs along densely packed directions $\langle 1\bar{2}10\rangle$. Plastic deformation can occur in the BCC lattice along all crystallographic planes belonging to the zone $\langle 111\rangle$. However, most of the sliding takes place along the planes $\{110\}$ and $\{112\}$ [23,24].

In a package consisting of α- and β-phase slats, elongation of the slats and reduction of their thickness is possible when sliding in the α-phase or along the base plane (0001) in

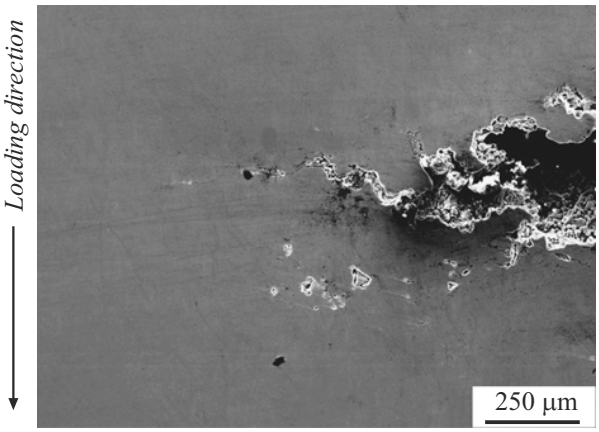

Figure 9. Pores in the VT8 alloy sample after loading with $V = (937 \pm 1.8)$ m/s at room temperature.

a direction parallel to the plane of habitus, or a prismatic plane coinciding with the plane of habitus. In the first case, the sliding in the β-phase will take place in the plane $\{110\}$ in a direction parallel to the plane of habitus, and in the second case along the plane $\{112\}$ coinciding with the plane of habitus. In areas of uniform deformation, the elongation of the slats and the decrease in their thickness are slightly noticeable, but it is clearly visible near the bands of deformation localization.

In the case of sliding in the αphase along the base plane (0001) in directions located at an angle to the plane of habitus, or in prismatic planes that do not coincide with the plane of habitus, part of the material passes into neighboring slats. This transition is observed in the form of the appearance of serration at the boundaries of the slats due to the different contrast of the α and β-phases in optical and SEM images. Sliding along these planes does not lead to localization of plastic deformation.

Conclusion

Stress wave profiles were obtained in this study in Ti6Al-3Mo titanium alloy samples in the impact load range from 4.6 to 13.2GPa, where the effects associated with elastic-viscous plastic deformation are most fully traced. Based on the obtained profiles, the following

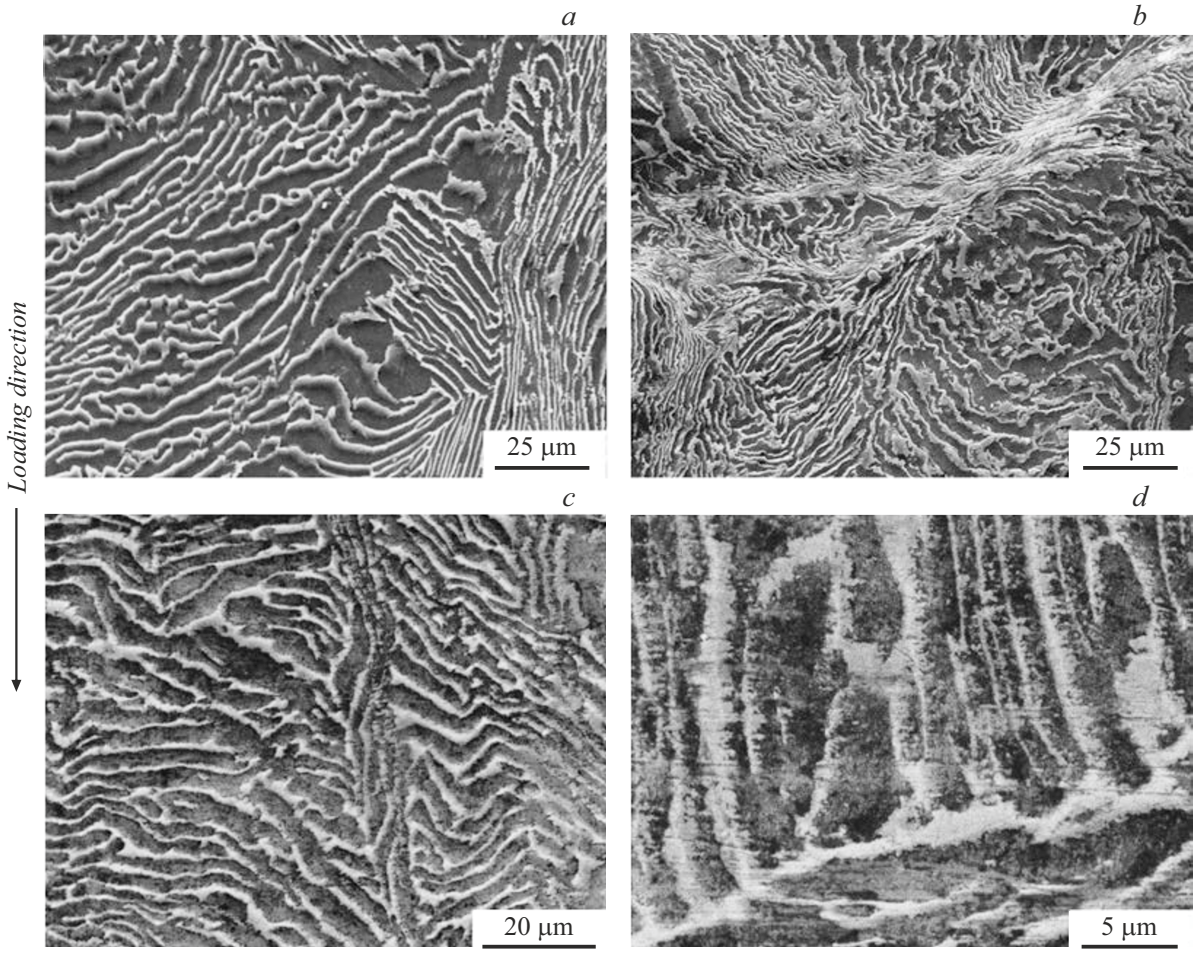

Figure 10. VT8 alloy structure after various loading modes: *a* — $V = (530 \pm 1.1)$ m/s, room temperature; *b* —$V = (532 \pm 1.1)$ m/s, $T = 400\,^{\circ}$C; *c*, *d* — $V = (937 \pm 1.8)$ m/s, room temperature.

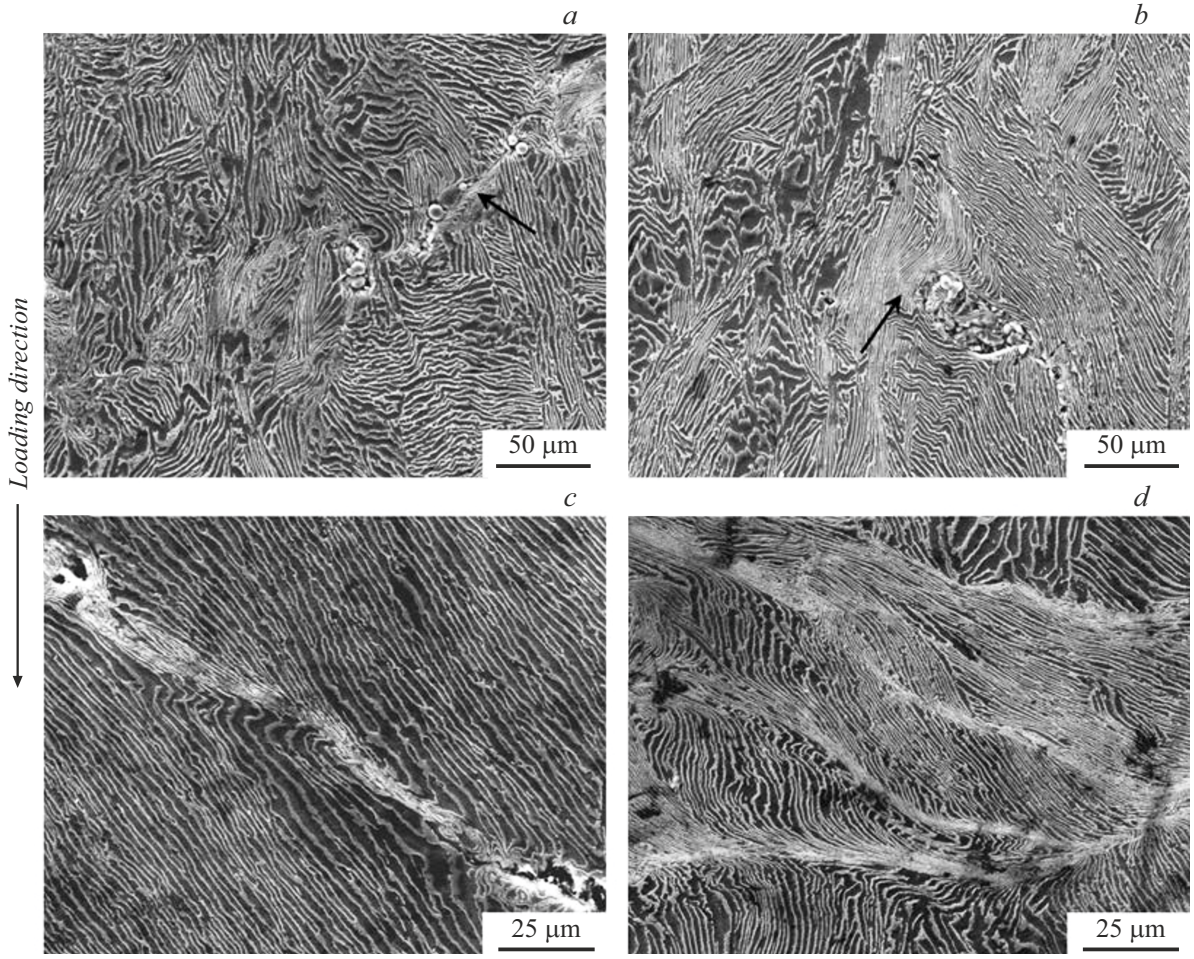

Figure 11. Deformation localization bands in the VT8 alloy sample after various loading modes: *a* — $V = (537 \pm 1.1)$ m/s, $T = -80\,^{\circ}$C; *b* — $V = (530 \pm 1.1)$ m/s, room temperature; *c*, *d* — $V = (532 \pm 1.1)$ m/s, $T = 400\,^{\circ}$C.

Microhardness of VT8 alloy samples after various loading modes

Loading mode	H_μ, MPa
$V = (537 \pm 1.1)$ m/s (6.2 GPa), $T = -80\,^{\circ}$C	3898 ± 54
$V = (530 \pm 1.1)$ m/s (6.1 GPa), room temperature	3883 ± 73
$V = (532 \pm 1.1)$ m/s (6.15 GPa), $T = 400\,^{\circ}$C	3826 ± 72
$V = (937 \pm 1.8)$ m/s (11.2 GPa), room temperature	3791 ± 64

were determined: the dependence of Hugoniot's elastic limit on the distance traveled by the wave in the material, $\sigma_{\mathrm{HEL}} = 2.86(h)^{-0.06}$, and the dependence of the deflection strength on the deformation rate in the rarefaction wave, — $\sigma_{\mathrm{HEL}} = 2.86(\varepsilon)^{0.046}$. As the material heats up, its dynamic strength and Hugonio's elastic limit decrease.

At a shock wave pressure above 11.7 GPa, there is a delay in the release of the deflection pulse onto the free surface of the sample, which indicates the presence of a $\alpha \rightarrow \omega$-phase transition, which is also accompanied by an increase in deflection strength.

The results of metallographic studies show that deflection fracture occurs through the formation of both deflection microcracks resulting from the nucleation and growth of small pores, and microcracks having a shear nature.

It is established that, under the realized loading conditions, high-speed plastic deformation is carried out by sliding. There is completely no twinning.

Along with homogeneous deformation, there is a localization of deformation, the maximum intensity of which is observed when loading a sample initially heated to $T = 400\,^{\circ}$C.

Acknowledgments

The work was performed using the equipment of the Shared Research Facility „Test Center for Nanotechnology and Advanced Materials“ Institute of Metal Physics, Ural Branch of RAS.

Funding

The study was conducted under the state assignment of the Ministry of Education and Science of the Russian Federation for the Institute of Metal Physics, Ural Branch of the Russian Academy of Sciences

Conflict of interest

The authors declare that they have no conflict of interest.

References

[1] S.V. Razorenov, A.V. Utkin, G.I. Kanel, V.E. Fortov, A.S. Yarunichev, K. Baumund, H.U. Karow. High Press. Res., **13**, 367 (1995). DOI: 10.1080/08957959508202588
[2] C.W. Greeff, D.R. Trinkle, R.C. Albers. J. Appl. Phys., **90**, 2221 (2001). DOI: 10.1063/1.1389334
[3] A.I. Petrov, M.V. Razuvaeva. Tech. Phys., **48** (6), 714 (2003).
[4] G.I. Kanel, S.V. Razorenov, E.B. Zaretsky, B. Herrman, L. Mayer. FTT, **45** (4), 625 (2003) (in Russian).
[5] A. Dobromyslov, N. Taluts., E. Kozlov. High Press. Res., **33**, 124 (2013). DOI: 10.1080/08957959.2012.758721
[6] V.A. Borisenok, M.V. Zhernokletov, A.E. Kovalev, A.M. Podurets, V.G. Simakov, M.I. Tkachenko. Combustion, Explosion and Shock Waves, **50** (3), 346 (2014). DOI: 10.1134/S0010508214030137
[7] G.I. Kanel, S.V. Razorenov, G.V. Garkushin. J. Appl. Phys., **119**, 185903 (2016). DOI: 10.1063/1.4949275
[8] G.I. Kanel, S.V. Razorenov, G.V. Garkushin, A.V. Pavlenko, S.N. Malyugina. FTT, **58** (6), 1153 (2016) (in Russian).
[9] G.I. Kanel, G.V. Garkushin, A.S. Savinykh, S.V. Razorenov, J. Experimental Theor. Phys., **127** (2), 337 (2018). DOI: 10.1134/S1063776118080022
[10] A.V. Pavlenko, A.V. Dobromyslov, N.I. Taluts, S.N. Malyugina, S.S. Mokrushin. Phys. Metals Metallography, **122** (8), 794 (2021). DOI: 10.1134/S0031918X2108010X
[11] A.V. Pavlenko, A.V. Dobromyslov, N.I. Taluts, S.N. Malyugina, S.S. Mokrushin. Mater. Today Commun., **31**, 103245 (2022).
[12] Yu.I. Mescheryakov, A.K. Divakov, N.I. Zhigacheva. Int. J. Shock Waves., **10**, 43 (2000).
[13] G.I. Kanel, G.V. Garkushin, S.V. Razorenov. ZhTF, **86** (8), 111 (2016) (in Russian) (in Russian).
[14] Y. Ren, J. Lin. Metals Mater. Intern., **27**, 4357 (2021). DOI: 10.1007/s1254 0-020-00721 -w
[15] P.S. Follansbee, G.T. Gray. Met. Trans. A, **20A**, 863 (1989).
[16] A.V. Pavlenko, S.I. Balabin, O.E. Kozelkov, D.N. Kazakov. Instruments and Experimental Techniques, **56** (4), 482 (2013). DOI: 10.1134/S0020441213040088
[17] A.V. Pavlenko, S.N. Malyugina, V.V. Pereshitov, I.N. Lisitsina. PTE, **2**, 127 (2013) (in Russian). DOI: 10.7868/S0032816213020122
[18] S.S. Mokrushin, N.B. Anikin, S.N. Malyugina, A.V. Pavlenko, A.A. Tyaktev. Instruments and Experimental Techniques, **57** (4), 475 (2014). DOI: 10.1134/S0020441214030075
[19] G.I. Kanel. PMTF, **42** (2), 194 (2001) (in Russian).
[20] Yu.V. Milman, I.V. Goncharova. Usp. Fiz. Met.-Prog. Phys. Met., **18**, 265 (2017). (in Russian).
[21] S.V. Zherebtsov, G.S. Dyakonov, G.A. Salishchev, A.A. Salem, S.L. Semiatin, Metall. Mater. Trans. A, **47**, 5101 (2016).
[22] U. Zwicker. *Titan und Titanlegirungen* (Springer-Verlag, Berlin, Heidelberg, NY., 1974)
[23] B.A. Kolachev. *Fizicheskoe materialovedenie titana* (Metallurgiya, M., 1976) (in Russian).
[24] R.W.K. Honeycombe. *The plastic deformation of metals* (Edward Arnold, London, 1968)

Translated by A.Akhtyamov